プロジェクト名：結晶Ｓｉ/有機ハイブリッド太陽電池の高効率化に関する研究
代表者：氏　名（所属・職名）　白井　肇（理工研・教授）

Effects of molybdenum oxide molecular doping on the chemical structure of poly(3,4-ethylenedioxythiophene):poly(stylenesulfonate) and on carrier collection efficiency of c-Si/PEDOT:PSS heterojunction solar cells

The effects of MoO_3 molecular doping in poly(3,4-ethylenedioxythiophene):poly(stylenesulfonate) (PEDOT:PSS) on the chemical structure and, in turn, on the carrier collection efficiency of c-Si/PEDOT:PSS heterojunction solar cells are demonstrated. Scanning electron microscopy revealed that the hydrophilic PSS polymer chain was intercalated into the interlayer van der Waals gap of MoO_3 flake sheets, which modified the chemical structure of PEDOT:PSS. MoO_3 exhibited intense photoluminescence in the 350-550 nm region, which enhanced the carrier collection efficiency of c-Si/PEDOT:PSS heterojunction solar cells with no significant changes. These findings suggest that the intense photoluminescence of MoO_3 and its light wavelength conversion contribute to the increased carrier collection efficiency.

1. Introduction

There has been tremendous interest in developing next-generation photovoltaics based on advanced materials such as quantum dots, semiconducting nanostructures and conjugated polymers.[1-3] Crystalline silicon (c-Si) remains the basic material for high-efficiency stable photovoltaics, and it has recently been demonstrated that Si nanowire junctions and Si wire arrays from catalytic growth or electrochemical etching can improve light absorption.[4-6] On the other hand, the integration of different nanostructures or polymers into Si-based photovoltaics has been explored widely, and many heterojunction structures have been reported, such as GaN nanorods epitaxially grown on n-type c-Si, InAs nanorods grown on p-type Si, and multiwalled nanotube (CNT) arrays grown in an anodized alumina template on Si substrates.[7-9]

Highly conductive poly(3,4-ethylenedioxythiophene):poly (stylenesulfonate) (PEDOT:PSS) is often used to modify indium tin oxide (ITO) electrodes owing to its superior injection/collection properties by secondary doping of novel reagents such as graphene, graphene oxide (GO), CNTs, and metal oxide particles.[10-13] It is also reported that PEDOT:PSS, GO, and metal oxide such as molybdenum trioxide (MoO_3) are good candidates for solution-processable hole-transporting materials that exhibits an intense photoluminescence (PL) emission in the 325-550 nm region and is expected to find application as a light wavelength conversion layer.[14-17] Furthermore, the MoO_3 layer would presumably generate a strong inversion in Si by electrostatic repulsion, as in the cases of dielectric SiO_x and Al_2O_3.[18-20] Thus, a high built-in voltage, V_{bi}, can be expected at the c-Si/PEDOT:PSS:MoO_3 composite interface.

In the present paper, we demonstrate the effect of luminescent MoO_3 molecular doping to conductive PEDOT:PSS on the chemical structure and external quantum efficiency (EQE) of n-type c-Si(100)/PEDOT:PSS heterojunction solar cells.

2. Experimental details

The c-Si wafer (CZ, 3-5 Ω·cm, 300 μm thickness) was cleaned by the RCA1 and RCA2 procedures. Highly conductive PEDOT:PSS (Clevios PH1000) with 5 wt% DMSO was used as a starting solution. MoO_3 (Kanto Kagaku Ltd. 99.99%) powder flake with an average size of 1.7 μm were used as a dopant. PEDOT:PSS:MoO_3 composite solutions with different MoO_3/(PEDT:PSS+MoO_3) (1, 3, 10, and 30 wt%) were stirred for 1h. As the PEDOT:PSS:MoO_3 solution was then stirred for 1h. Here, as the PEDOT:PSS solid content of PH1000 is around 1%,[21] the dry weight ratios of MoO_3/PEDOT:PSS composite thin films were much higher than the values reported in present paper, for example, in the case of the 1 wt% composite, the real dry weight ratio of MoO_3/PEDOT:PSS was almost unity. A thin film was formed by spin-coating the precursor solution on RCA-cleaned c-Si wafers at 1000 rpm for 60 s, followed by thermal annealing at 140˚C for 30 minutes. Finally, a top Ag grid electrode was fabricated by pattern printing. The PEDOT:PSS:MoO_3 composite films were characterized using scanning electron microscopy (SEM), energy dispersive X-ray spectroscopy (EDX), X-ray photoelectron spectroscopy (XPS), and spectroscopic ellipsometry (SE). The PL spectra were measured using FluoroMax-3 (Horiba Jovin-Yvon) spectrophotometer.

3. Results and discussion

Figure 1(a) shows the SEM image of MoO_3 particles in conductive PEDOT:PSS. The inset shows the crystal structure of MoO_3. MoO_3 exhibits a layered structure consisting of vertex-sharing chains of distorted MoO_6 octahedra that share edges with two similar chains to form layers. The distortion gives rise to very short "Mo=O" bonds at the apical octahedral positions that terminate the top and bottom of the double-octahedral oxide sheets.

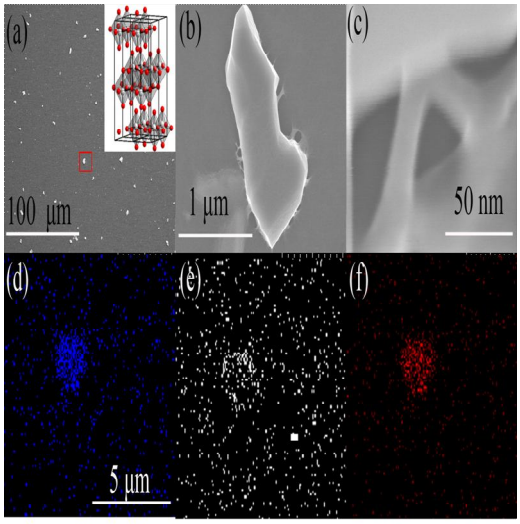

FIG. 1 SEM images (a-c) and EDX maps (d-f) (corresponding to the circled region in Fig. 1 (a)) of MoO_3 particle in PEDOT:PSS. Inset illustrates crystal structure of MoO_3 where red and gray spheres denote O and Mo atoms, respectively, (b) and (c) show the novel hair-like structure. (d), (e), and (f) are the EDX maps for Mo, O, and S, respectively, in MoO_3 doped PEDOT:PSS.

The resultant two-dimensionally bonded layers are stacked in a staggered arrangement and held together by weak van der Waals forces. A variety of large guest species can be intercalated into the interlayer van der Waals gap.[22] The SEM image shows a hairlike projections around the MoO_3 flake sheets with an average diameter of 15~20 nm which is much smaller than the typical mean size of PEDOT particles embedded in PSS chains.[23] EDX maps of Mo, O, and S for the PEDOT:PSS:MoO_3 (3 wt%) composite are shown in Figs. 1(d)-(f). Notably, the EDX image of Mo was almost consistent with that of S despite the use of MoO_3, and even though S was distributed homogeneously. This implies that

the sulphur in PEDOT and/or PSS is coordinated preferentially in MoO_3 particle. In addition, the average *d* spacing of the collected composite powder, as calculated from the four 0*k*0 reflections in the XRD spectra, was 0.9-1.1nm, i.e., larger than that of pristine MoO_3 (0.6 nm). Furthermore, XPS revealed that the 3d binding energy corresponding to S=O in PSS decreased less for higher MoO_3 concentrations. These findings suggest that the concentration ratio of PEDOT to PSS increased. Thus, the PSS chain was intercalated into the MoO_3 flake sheet, modifying the chemical structure of PEDOT:PSS conjugated polymer.

Figure 2 shows the PL spectra of pristine MoO_3 and PEDOT:PSS:MoO_3 composite films at room temperature and the excitation PL (PLE) spectra for the 400 nm emission. Optical micrographs of PEDOT:PSS with and without MoO_3 doping are shown as well. An intense broad band PL emission at 350-500 nm having a maximum peak at around 390-400 nm was observed, and its intensity increased with MoO_3 doping concentration. Thus, the UV light at 310-345 nm was absorbed and efficiently showed an intense broadband PL emission at ~400 nm. In fact, the MoO_3-doped PEDOT:PSS micrograph was deep purple, owing to the intense PL emission at 350-550 nm from MoO_3. These results suggest that MoO_3 may potentially be used for absorbing light at short wavelengths and then emitting at longer wavelengths (350-550 nm), which would enhance the carrier collection efficiency of c-Si/PEDOT:PSS solar cells.

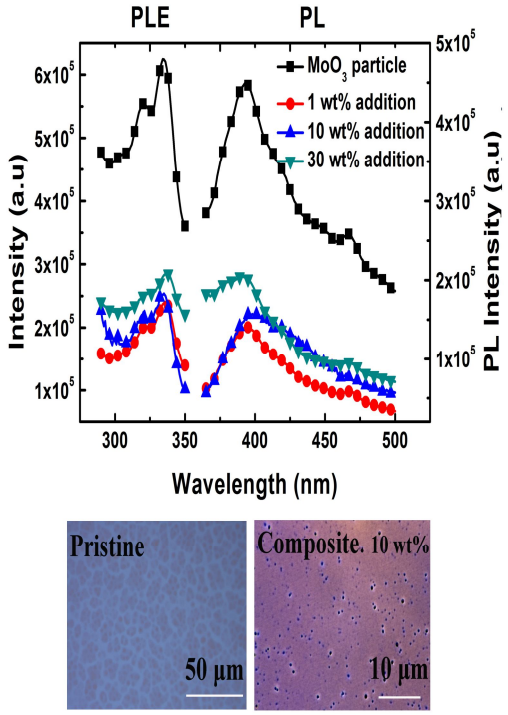

FIG. 2 PL and PLE spectra of MoO_3 doped PEDOT:PSS film under 400-nm excitation. The optical micrographs of PEDOT:PSS with and without 10 wt% MoO_3 doping are shown as well.

Figure 3(a) shows the current density-voltage (*J*-V) curves obtained under AM1.5 100 mW/cm^2 simulated solar light (Bunkoukeiki CEP-25BX) for c-Si(100)/PEDOT:PSS:MoO_3 composite heterojunction solar cells with different MoO_3 doping concentrations.. The inset is a schematic of a c-Si/organic heterojunction solar cell. The effective area of each cell was 5×5 mm^2. η was calculated via $\eta=V_{oc}J_{sc}FF/P_{in}$, where V_{oc} is the open-circuit voltage, J_{sc} is the short-circuit current density, *FF* is the fill factor, and P_{in} is the incident light power. *FF* is determined via $FF=(V_mJ_m)/(V_{oc}J_{sc})$, where V_m and J_m are, respectively, the voltage and current density in the maximum power in the fourth quadrant of the *J*-V curves. The reverse and forward dark currents were suppressed to below the values for a pristine PEDOT:PSS diode. η increased to 11.01% with a J_{sc} of 29.4 mA/cm^2, a V_{oc} of 0.552 V, and an *FF* of 0.683 at a MoO_3 concentration of 1 wt%.

J_{sc} increased with MoO_3 doping concentration up to 3 wt%. However, V_{oc} and *FF* decreased markedly with further increase in MoO_3 concentration, due to the increased series resistance, R_s. The $1/C^2$-V plot at 1 MHz also showed a relatively high V_{bi} of 0.9-1 eV, resulting in a higher V_{oc} than that of pristine PEDOT:PSS. The EQE and difference EQE (DEQE) spectra for solar cells with different MoO_3 doping concentrations are shown in Fig. 3(b). Here, the DEQE values are relative to that of a pristine c-Si/PEDOT:PSS solar cell, DEQE was found to be positive over the entire wavelength region of 350-1200 nm for a MoO_3 concentration of 1-3 wt%. At high MoO_3 doping concentrations of up to 10-30 wt%, DEQE was markedly enhanced in the 350-550 nm regions, with a shorter wavelength shift, but the values in the infrared region of 900-1200 nm were negative. It has been reported that polar solvent such as MeOH and ethylene glycol modify the chemical structure of PEDOT:PSS and that the phase separation of PEDOT-PSS enhances the hole mobility of PEDOT:PSS by increasing conduction path network of PEDOT chains.[24,25] These findings suggest that the increased EQE in the 350-550 nm region of c-Si/PEDOT:PSS:MoO_3 composite heterojunction solar cells is due to the PL emission of MoO_3.

The PLE and PL spectra of pristine MoO_3 are shown in Fig. 4(a). The EQE and DEQE spectra of c-Si/PEDOT:PSS solar cells with and without a 30 wt% MoO_3 doping and spectroscopic sensitivity of sunlight are also included. The PL spectra at 360-510 nm can be ascribed to the intense near-band-edge (NBE) emission due to the free-exciton recombination and visible light emission by transitions of excited optical centers in the deep levels (DLs). The UV absorption between 310-345 nm led to visible PL emission in the 360-510 nm range. This visible wavelength region corresponds to those of the increased DEQE for c-Si/PEDOT:PSS:GO composite solar cells.

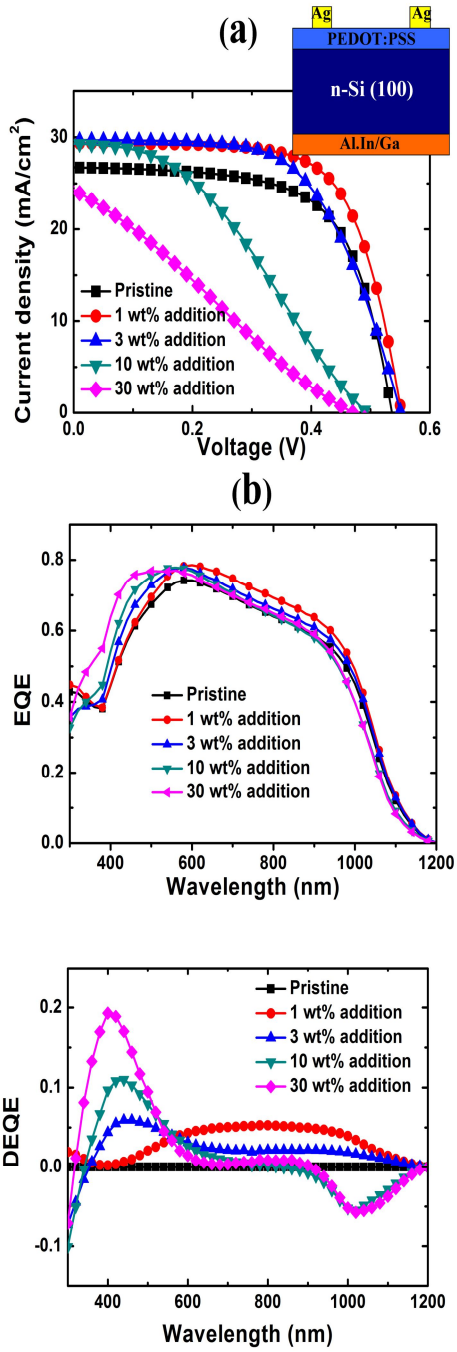

FIG. 3 (a): *J*-V curves for n-Si/PEDOT:PSS:MoO_3 composite heterojunction solar cells with different MoO_3 concentrations. Inset shows schematic of the device structure of c-Si/PEDOT:PSS:MoO_3 composite solar cells. (b): EQE and DEQE spectra for c-Si/PEDOT:PSS:MoO_3 composite heterojunction solar cells. DEQE values are relative to that of a pristine PEDOT:PSS solar cell.

The reflectance spectra for PEDOT:PSS:MoO_3 composite films, as determined by SE spectra analysis, are shown in Fig. 4(b). The reflectance spectra in the UV region corresponding to the absorption of c-Si decreased slightly by MoO_3 doping, but no significant changes were observed. AFM revealed that the degree of RMS roughness was 3-9 nm (5×5 μm^2), which is less than that of light trapping. Thus, the improved EQE in the

350-550 nm region does not result from MoO_3 acting as an anti-reflection layer but from the enhanced optical absorption in this region owing to the PL emission from MoO_3. The RMS roughness of the thin film examined by AFM was around 9 nm, up to a MoO_3 doping concentration of 10 wt%, which is negligibly small for a light-harvesting structure, as compared with that of textured Si(100). However, the EQE in the infrared region of 900-1200 nm deteriorated at a MoO_3 doping concentration above 10 wt% due to the increased optical reflectivity.

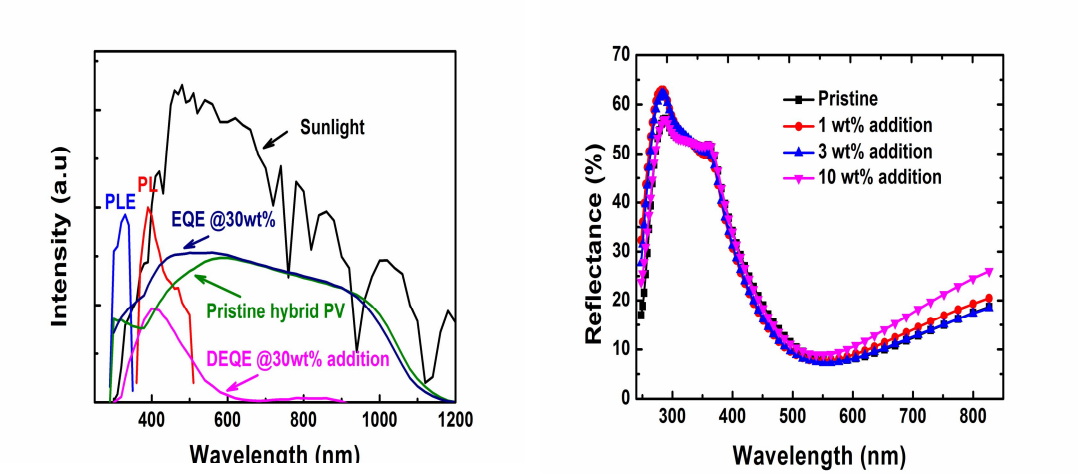

FIG. 4 (a) The PLE and PL spectra of pristine MoO_3. The EQE, DEQE of c-Si/PEDOT:PSS solar cells and spectroscopic sensitivity of sunlight are also shown. **(b)** Reflectance spectra for c-Si(100)/PEDOT:PSS:MoO_3 composite solar cells with different MoO_3 doping concentrations. All PEDOT:PSS:MoO_3 layer thicknesses were 100 nm.

4. Conclusions

We studied the effect of MoO_3 molecular doping to conductive PEDOT:PSS on the chemical structure and photovoltaic properties of c-Si/PEDOT:PSS heterojunction solar cells. The MoO_3 molecular doping modified the chemical structure of PEDOT:PSS by the intercalation of PSS into the van der Waals gap of MoO_3 sheets. These changes enhanced the photovoltaic performance of the c-Si/PEDOT:PSS solar cells. η increased up to 11.0%. The UV absorption and intense PL emission at 350-550 nm increased the carrier collection efficiency in c-Si/PEDOT:PSS heterojunction solar cells.

References

1. N. S. Lewis, Science **315**, 798 (2007).
2. A. G. Pattantyus-Abraham, I. J. Kramer, A. R. Barkhouse, X. Wang, G. Konstantatos, R. Debanth, L. Levina, I. Raabe, M. K. Nazeeeruddin, M. Gratzel, E. H. Sargent, ACS Nano **4**, 3374 (2010).
3, W. A. Tisdale, K. J. Geiser, A. P. Alivisatos, Science **310**, 462 (2005).
4. B. Tian, X. Zheng, T. J. Kempa. Y. Fang, N. Yu, G. Yu, J. Huang, C. M. Lieber, Nature **339**, 885 (2007).
5. V. Sivakaov, G. Andra, A. Gawlik, A. Berger, J. Plentz, F. Falk, S. H. Christiansen, Nan Lett. **9**, 1549 (2009).
6. S. W. Boettcher, J. M. Spurgeon, M. C. Putnam, E. L. Warren, D. B. Turner-Evans, M. D. Kelzenberg, J. R. Maiolo, H. A. Atwater, N. S. Lewis, Science **327**, 185 (2010).
7. Y. B. Tang, Z. H. Chen, H. S. Song, C. S. Lee, H. T. Cong, H. M. Cheng, W. J. Zhang, I. Bello, S. T. Lee, Nano Lett. **8**, 4191 (2008).

8. W. Wei, X. -Y. Bao, C. Soci, Y. Ding, Z.-L. Wang, D. Wang, Nano Lett. **9**, 2926 (2009).
9. M. B. Tzolov, T. -F. Kuo, D. A. Straus, A. Yin, J. Xu, J. Phys. Chem. C **111**, 5800 (2009).
10. J-H Jung, J-J Zeng, Y-U. Su, and Y-J Lin, Appl. Phys. Lett. **100**, 153509 (2012).
11. Y-J. Lin and Y-C. Su, J. Appl. Phys. **111**, 073712 (2012).
12. B. Yin, Q. Liu, X. Wu, Z. Liu. Y. Hua, S. Yin, and Y. Chen, J. Nanosci. & Nanotech. **10**, 1934 (2010).
13. I. Khatri, Q. Liu, R. Ishikawa, K. Ueno, and H. Shirai, Phys. Status Solidi. C, **9**, 2134–2137 (2012).
14. S. Kato, R. Ishikawa, Y. Kubo, H. Shirai, and K. Ueno, Jpn. J. Appl. Phys. **50**, 071604 (2012).
15. Q. Liu, F. Watanabe, A. Hoshino, R. Ishikawa, T. Gotou, K. Ueno, and H. Shirai, Jpn. J. Appl. Phys. **51**, 10NE22, (2012).
16. L. He, C. Jiang, H. Wang, D. Lai, and Rusli, Appl. Phys. Lett. **100**, 073503 (2012).
17. Q. Liu, H. Ino, Z. Tang, R. Ishikawa, K. Ueno, and H. Shirai, Appl. Phys. Lett. **100**, 183901 (2012).
18. B. Hoex, S. B. S. Heli, E. Langereis, M.C. M van de Sanden, and W. M. M. Kessels, J.Appl. Phys. **104**, 114703 (2008).
19. B. Hoex, J. J. H. Gielis, M.C. M. van de Sanden, and W. M. M. Kessels, Appl. Phys. Lett. **89**, 042112 (2006).
20. A. S. Erickson, N. K. Kedem, A. E. Haji-Yahia, and D. Cahen, Appl. Phys. Lett. **101**, 233901 (2012).
21. This information was cited from following website: http://clevios.com/media/webmedia_local/media/datenblaetter/81076210_Clevios_PH_1000_20101222.pdf
22. T. A. Kerr, H. Wu, and L. F. Nazar, Chem Mater. **8**, 2005 (1996).
23. A. M. Nardes, M. Kemerink, R. A. J. Janssen et al., Adv. Mater, **19**(9), 1196-1200, 2007.
24. M. Yamashita, C. Otani, M. Shimizu, and H. Okuzaki, Appl. Phys. Lett. **99**, 143307 (2012).
25. Q. Liu, I. Khatri, R. Ishikawa, K. Ueno, and H. Shirai, to be published in Appl. Phys. Lett.